THE JOURNAL OF BIOLOGICAL CHEMISTRY Vol. 280, No. 32, Issue of August 12, pp. 29088–29095, 2005

Printed in U.S.A.

Architecture of the Human Ndc80-Hec1 Complex, a Critical Constituent of the Outer Kinetochore*

Received for publication, April 14, 2005, and in revised form, May 31, 2005
Published, JBC Papers in Press, June 16, 2005, DOI 10.1074/jbc.M504070200

Claudio Ciferri‡§, Jennifer De Luca¶, Silvia Monzani‡, Karin J. Ferrari‡, Dejan Ristic‖, Claire Wyman‖, Holger Stark‡‡, John Kilmartin§§, Edward D. Salmon¶, and Andrea Musacchio‡§¶¶**

*From the ‡Department of Experimental Oncology, European Institute of Oncology, Via Ripamonti 435, 20141 Milan, Italy, the §Italian Foundation for Cancer Research (FIRC) Institute of Molecular Oncology Foundation, Via Adamello 16, 20139 Milan, Italy, the ¶Department of Biology, University of North Carolina, Chapel Hill, North Carolina 27599, the ‖Department of Radiation Oncology, Daniel Den Hoed Cancer Center and the **Department of Cell Biology and Genetics, Erasmus Medical Center, P. O. Box 1738, 3000 DR, Rotterdam, The Netherlands, the ‡‡Max Planck Institute for Biophysical Chemistry, Am Fassberg 11, 37077 Goettingen, Germany, and the §§Medical Research Council Laboratory of Molecular Biology, Hills Road, Cambridge CB2 2QH, United Kingdom*

The Ndc80 complex is a constituent of the outer plate of the kinetochore and plays a critical role in establishing the stable kinetochore-microtubule interactions required for chromosome segregation in mitosis. The Ndc80 complex is evolutionarily conserved and contains the four subunits Spc24, Spc25, Nuf2, and Ndc80 (whose human homologue is called Hec1). All four subunits are predicted to contain globular domains and extensive coiled coil regions. To gain an insight into the organization of the human Ndc80 complex, we reconstituted it using recombinant methods. The hydrodynamic properties of the recombinant Ndc80 complex are identical to those of the endogenous HeLa cell complex and are consistent with a 1:1:1:1 stoichiometry of the four subunits and a very elongated shape. Two tight Hec1-Nuf2 and Spc24-Spc25 subcomplexes, each stabilized by a parallel heterodimeric coiled coil, maintain this organization. These subcomplexes tetramerize via an interaction of the C- and N-terminal portions of the Hec1-Nuf2 and Spc24-Spc25 coiled coils, respectively. The recombinant complex displays normal kinetochore localization upon injection in HeLa cells and is therefore a faithful copy of the endogenous Ndc80 complex.

Kinetochores mediate the attachment of chromosomes to microtubules of the mitotic spindle (1, 2). The kinetochores of *Saccharomyces cerevisiae* assemble on ~150-base pair-long centromeric DNA wrapped around a specialized nucleosome containing Cse4, a histone H3 variant known as CENP-A in higher eukaryotes (3). These kinetochores become attached to the plus end of a single microtubule and are estimated to contain at least 60 different proteins in several subcomplexes (3). Together, these subcomplexes produce stable DNA-microtubule bridges and control the spindle assembly checkpoint. The latter delays anaphase sister chromatid separation until all chromosomes have achieved bio-orientation by their sister kinetochores becoming attached to microtubules from opposite poles (4).

* This work was supported by grants from the Italian Association for Cancer Research (AIRC), the Italian Ministry of Health, and the Human Frontier Science Program. The costs of publication of this article were defrayed in part by the payment of page charges. This article must therefore be hereby marked "*advertisement*" in accordance with 18 U.S.C. Section 1734 solely to indicate this fact.

¶¶ To whom correspondence should be addressed. Tel.: 39-02-57489829; Fax: 39-02-57489851; E-mail: andrea.musacchio@ifom-ieo-campus.it.

Human centromeres extend over millions of base pairs, and the compaction of centromeric chromatin is essential for their viability (1, 2). Recent proteomic efforts in different organisms have clarified that despite significant differences in centromere complexity, most kinetochore proteins are conserved from yeast to humans (5–12). Thus, complex kinetochores might be assembled from building blocks that are structurally related to that of *S. cerevisiae*. By electron microscopy the vertebrate kinetochore appears as a multilayered structure with an inner core embedded in the centromeric chromatin and connected by a 40-nm fibrous gap to a 40-nm thick outer plate. A 150-Å-thick dynamic structure known as the fibrous corona extends outward from the outer plate (13–18). Vertebrate kinetochores bind multiple microtubules (from 15 to 30) whose plus ends terminate within the outer plate (1, 13).

The dynamic properties of microtubule-kinetochore interfaces are thought to be responsible for chromosome movement in mitosis (19, 20). Although the mechanisms leading to the formation of microtubule-kinetochore interfaces remain poorly understood, the Ndc80 protein has emerged as a potentially critical player in this process. In budding yeast Ndc80 is part of the Ndc80 complex, which also contains Nuf2, Spc24, and Spc25 (10, 21, 22). This quaternary organization is conserved in the *Xenopus* and human complexes (23–25). The human homologue of Ndc80 is referred to as Hec1, which stands for highly enhanced in cancer cells 1 (26), and we will refer to Hec1 as a subunit of the human Ndc80 complex. Antibodies to Hec1 localize to the outer plate of HeLa cell kinetochores where the plus ends of kinetochore microtubules are anchored (27–30). Depletion or inactivation of subunits of the Ndc80 complex by several methods invariably results in severe problems of chromosome congression and lack of poleward forces at the kinetochore (reviewed in Refs. 19 and 20).

There has been some controversy as to whether the defective chromosome congression phenotype resulting from depletion of Ndc80 is caused by a defect in kinetochore-microtubule attachment. Depletion of Hec1 or Spc25 by RNA interference in HeLa cells resulted in a failure of chromosomes to congress to the spindle equator, but the existence of kinetochore-microtubule connections that resisted short cold or calcium treatments and the localization of the microtubule plus end-binding protein EB1 at the kinetochore-microtubule interface suggested that stable kinetochore-microtubule interactions may form in these cells (23, 31).

Recent studies, however, concluded that cells depleted of

Hec1 or Nuf2 display a damaged outer kinetochore, coupled to a dramatic decrease in the number of microtubules embedded in the outer kinetochore surface and to a failure to accumulate cold-stable microtubules (27–30). Thus, the Ndc80 complex might be essential for the formation of stable kinetochore-microtubule interactions, suggestive of a direct role in microtubule binding or, alternatively, a role in a kinetochore assembly pathway, the impairment of which abrogates recruitment of other proteins required for microtubule binding. Indeed, the depletion/inactivation of the Ndc80 complex causes a corresponding kinetochore depletion or reduction of a group of proteins normally localized at or in the corona peripheral to the kinetochore outer plate, including the motor proteins dynein/dynactin and the spindle assembly checkpoint proteins Mps1, Mad1, Mad2, Zw10, and Rod. However, peripheral checkpoint proteins and motor proteins such as Bub1, BubR1, and CENP-E retain an essentially normal kinetochore localization under these conditions (23–25, 28–33). In summary, the Ndc80 complex plays a direct role in stabilizing the kinetochore-microtubule interface and in controlling the localization of a subset of proteins at or in the corona peripheral to the kinetochore outer plate, although its precise function in these processes remains unclear. The complexity of the putative microtubule-kinetochore interface is underscored by the recent discovery that the Ndc80 complex is part of an evolutionarily conserved protein assembly also containing the Mtw1-Mis12 complex and other proteins such as Zwint-1 and Spc105 (7–11). The role of the Ndc80 complex as a direct or indirect kinetochore receptor for Mps1, Mad1, Mad2, Zw10, and Rod might also explain the effects of Ndc80 depletion on the spindle assembly checkpoint. These effects range from complete inactivation to sustained activation followed by cell death, with a discrepancy that might be explained by the penetrance of the depletion phenotype (23–25, 28–35).

Because of the complexity of kinetochore structure, the development of *in vitro* approaches using reconstituted kinetochore complexes will be invaluable to elucidate the mechanism of formation of kinetochore-microtubule interfaces. Here, we describe a step in this direction represented by the reconstitution and characterization of the human Ndc80 complex. We show that the reconstituted complex forms a quaternary assembly whose biophysical, biochemical, and biological properties are indistinguishable from those of the endogenous complex.

MATERIALS AND METHODS

Cloning, Expression, and Purification of Hec1 Complex Constructs—All constructs for human Spc24, Spc25, Nuf2, and Hec1 subunits were generated by PCR using a human fetal thymus cDNA library (Invitrogen). Spc24, Spc25, Nuf2, and Hec1 sequences were subcloned in a modified pGEX-6P vector (pGEX-6P-2RBS) to support dicistronic expression. All constructs were sequenced. Protein expression in *Escherichia coli* strain BL21 (DE3) was induced with 400 μM isopropyl-β-D-thiogalactopyranoside. Expression was continued for ~12–16 h at 18–20 °C. Cells were harvested by centrifugation at 4,000 rpm for 15 min in a Beckman JLA 10.5 rotor and resuspended in 30–40 ml of lysis buffer (50 mM Tris-HCl, pH 7.6, 600 mM NaCl, 10% glycerol, 1 mM EDTA, and 1 mM dithiothreitol supplemented with Complete protease inhibitor mixture from Roche Molecular Biochemicals) per liter of *E. coli* culture. After sonication, the lysates were cleared by centrifugation at 40,000 rpm for 45–60 min using a 55.1 Ti rotor. Glutathione *S*-transferase (GST)[1]-Spc24-Spc25 and GST-Nuf2-Hec1 were purified using glutathione-agarose beads (Amersham Biosciences). After 2–3 h of agitation at 4 °C, beads were washed with 30 volumes of lysis buffer and equilibrated with 30 volumes of cleavage buffer (50 mM Tris-HCl, pH 7.6, 150 mM NaCl, 1 mM EDTA, and 1 mM dithiothreitol). The Spc24-Spc25 subcomplex was cleaved from GST with 10 units of PreScission protease (Amersham Biosciences) per milligram of substrate for 16 h at 4 °C. Simultaneously, the GST-Nuf2-Hec1 complex was expressed and purified as described above and incubated with the flow through of PreScission cleavage of the GST-Spc24-Spc25 complex. After forming a quaternary Ndc80 complex, PreScission protease was added to remove the GST moiety from Nuf2. The quaternary complex was collected in the flow through, concentrated up to 5 mg/ml by Vivaspin (molecular weight cut-off 30,000) and loaded onto a Superose 6 column equilibrated with size exclusion chromatography (SEC) buffer (50 mM Tris-HCl pH 7.6, 600 mM NaCl, 1 mM EDTA, 1 mM dithiothreitol, and 5% glycerol). The final yield was estimated at ~0.1 mg of pure complex per liter of bacteria. For binding assays and analytical SEC we also created the vectors pGEX-6P-Nuf2-(1–137), pGEX-6P-Nuf2-(1–386), pGEX-6P-Nuf2-(387–464), pAM3-His$_6$-Hec1-(1–230), pAM3-His$_6$-Hec1-(1–445), pAM3-His$_6$-Hec1-(446–642), pGEX-6P-2RBS-Spc24-(1–131)·Spc25-(1–144), pGEX-6P-2RBS-hSpc24-(1–131)·hSpc25-(145–224), pGEX-6P-2RBS-hSpc24-(132–197)·hSpc25-(1–144), pGEX-6P-2RBS-hSpc24-(132–197)·hSpc25-(145–224), pGEX-6P-2RBS-GST-Nuf2-(1–386)·Hec1-(1–445), and pGEX-6P-2RBS-GST-Nuf2-(387–464)·Hec1-(446–642). These vectors were used for protein expression and purification essentially as described above for the quaternary Ndc80, except that the salt concentrations of buffers were usually kept at 300 mM NaCl.

Hydrodynamic Analysis—Analytical SEC was performed on a SMART system (Amersham Biosciences) using a Superdex 200 PC 3.2/30 column (Amersham Biosciences). Elution volumes of bovine thyroglobulin, rabbit aldolase, hen egg albumin, and ribonuclease A were plotted against their known Stokes radii (82.55, 46.15, 30.5, and 16.4 Å, respectively) to generate a calibration curve ($R^2 = 0.98$) from which the Stokes radius of Ndc80 was determined. For glycerol velocity gradients, samples were loaded directly onto 12-ml 5–40% glycerol gradients prepared by layering eight 1.5-ml aliquots of gradient buffer (50 mM Tris-HCl, pH 7.6, 150 mM NaCl, 1 mM dithiothreitol, 1 mM EDTA, and 10 mM phenylmethylsulfonyl fluoride) containing a decreasing glycerol concentration. Centrifugation was protracted for 48 h at 40,000 rpm on a Beckman SW41Ti swinging bucket rotor at 4 °C. The gradient was fractionated in 300-μl fractions, the content of which was visualized by SDS-PAGE after precipitation with trichloroacetic acid. Chymotrypsinogen A (25-kDa monomer, 2.58 S), bovine serum albumin (60-kDa monomer, 4.22 S), aldolase (158-kDa tetramer, 7.4 S), and catalase (240-kDa tetramer, 11.3 S) were also analyzed and their elution plotted against the known Svedberg coefficient. The resulting calibration curve ($R^2 = 0.97$) was used to determine the sedimentation coefficient (**s**) of the Ndc80 complex. The molecular weight was calculated from the Stokes radius (**a**) in Ångstroms and from **s** according to the equation molecular weight = α**as** (36), where $\alpha = (6\pi\eta_0 N)/(1 - \upsilon\rho)$, N is Avogadro's number (6.02×10^{23}), η_0 is the viscosity of medium (g/(cm·s)), ρ is the density of the medium (g/ml), and υ is the partial specific volume of the analyzed particle (ml/g). Because η_0 and ρ values change according to the buffer composition and υ depends on the amino acidic composition, the α value was determined by plotting the molecular weights of standard proteins against their **a** × **s** values. The axial ratio of the prolate ellipsoid of rotation was calculated as described (37).

GST Pull-down Experiments—GST fusion proteins were expressed and purified as described above. Binding of the GST fusion proteins to their interacting partners fused to a hexahistidine (His$_6$) tag was tested by anti-His tag Western blotting (WB). Each interaction was verified by at least three independent experiments.

Binding Assay and Alexa Fluor 488 (Alexa) Labeling—Hec1-(1–445)·Nuf2-(1–386), Hec1-(446–642)·Nuf2-(387–464), Alexa-Spc24-(1–197)·Spc25-(1–224), and Alexa-Spc24-(70–197)·Spc25-(57–224) subcomplexes were analyzed on a Superdex™ 200 PC 3.2/30 SEC column. 35-μl fractions were collected, and their contents were analyzed by SDS-PAGE and Coomassie staining. To test the interaction of the the subcomplexes, Hec1-(1–445)·Nuf2-(1–386) or Hec1-(446–642)·Nuf2-(387–464) were incubated for 2 h on ice with Alexa-Spc24-(1–197)·Spc25-(1–224) or Alexa-Spc24-(70–197)·Spc25-(57–224). The reaction mixes were analyzed by SEC as described above. Proteins were labeled with Alexa-488 succimidyl ester reactive dye (Molecular Probes, Inc.) as described (38).

Cell Culture, Injections, and Microscopy—HeLa cells were maintained in Dulbecco's modified Eagle's medium (Invitrogen) containing 10% fetal bovine serum and antibiotic/antimycotic solution and cultured in a 37 °C, 5% CO_2 incubator. The culture of PtK1 cells and microinjection techniques were described previously (39). For microinjection experiments, cells were grown on acid-washed coverslips in 35-mm Petri dishes. Cells were microinjected with ~1–5% cell volume of Alexa-labeled Spc24-Spc25 protein complex (at 86 μM needle concentration) or Alexa-labeled Hec1 complex (at 26 μM needle concentration) and then placed in Leibovitz's dye-free L-15 medium, pH 7.2 (Sigma), supplemented with 7 mM Hepes,

[1] The abbreviations used are: GST, glutathione *S*-transferase; Alexa, Alexa Fluor 488; h (prefix), human; SEC, size exclusion chromatography; SFM, scanning force microscopy; WB, Western blotting.

10% fetal bovine serum, an antibiotic/antimycotic solution, 4.5 g/liter glucose, and 0.45 units/ml Oxyrase (Oxyrase Inc., Mansfield, OH). HeLa cells injected with the Alexa-Spc24-Spc25 complex or the Alexa-Ndc80 complex were fixed with 4% paraformaldehyde and subsequently permeabilized with 1% Triton X-100. Alexa-Spc24–25-injected cells were incubated overnight at 4 °C with Hec1 primary antibodies (Abcam, Cambridge, UK) at a dilution of 1:750; Alexa-Ndc80-injected cells were incubated with CREST serum (Antibodies Inc., Davis, CA) at a dilution of 1:2000. The secondary antibodies used were rhodamine Red-X anti-mouse for Alexa-Spc24-Spc25 injected cells and rhodamine Red-X anti-human for Ndc80 complex-injected cells. Images were obtained using a Nikon 100×, 1.4 numerical aperture planapochromat oil immersion lens on a spinning disc confocal fluorescence microscope. For live cell imaging, cells on coverslips mounted into Rose chambers were imaged as described above.

Scanning Force Microscopy—For imaging, 20 μl of a diluted Ndc80 complex reconstituted as described above was deposited on freshly cleaved mica. After ~30 s the mica was washed with water (glass-distilled; Sigma) and exposed to a stream of filtered air. Images were obtained on a NanoScope IV (Digital Instruments; Santa Barbara, CA) operating in tapping mode in air with a type E scanner. Silicon nanotips were from Digital Instruments (Nanoprobes).

RESULTS

Domain Structure of the Human Ndc80 Complex—To investigate the interactions connecting the four subunits of human Ndc80 we used a bacterial co-expression strategy. Dicistronic vectors were designed to express the first recombinant cistron as a C-terminal fusion to a His_6 tag or to GST. The second cistron was expressed as an untagged protein or as a His_6 tag fusion (when the first cistron was fused to GST). In co-expression experiments with the full-length proteins we determined that Nuf2-Hec1 and Spc24-Spc25 form two stable subcomplexes (see below). We exploited this observation to map the dimerization domains within each subcomplex by creating constructs expected to coincide with the predicted globular and coiled coil (40) regions of Nuf2, Hec1, Spc24, and Spc25 shown in Fig. 1*A*.

In a first set of experiments we tested the ability of His-Hec1-(1–445) to bind different regions of Nuf2 fused to GST. His-Hec1-(1–445) was co-expressed with GST, GST-Nuf2-(1–385), or GST-hNuf2-(386–464). Bacterial lysates were incubated with GSH-Sepharose, and any His-tagged Hec1 fusion protein bound to Nuf2 was detected by WB with an anti-His-tagged antibody. His-Hec1-(1–445) bound tightly to GST-Nuf2-(1–385) (Fig. 1*B*, *lane 6*) and not to GST or GST-hNuf2-(386–464) (*lanes 3* and *9*). This result identifies an interaction between the N-terminal regions of Nuf2 and Hec1.

Next, we co-expressed His-Hec1-(446–642) with GST, GST-Nuf2-(1–385), or GST-hNuf2-(386–464). Interestingly, we found a tight interaction between His-Hec1-(446–642) and GST-hNuf2-(386–464) (*lane 9*), whereas no binding was observed to GST or GST-Nuf2-(1–385) (*lanes 3* and 6). This experiment also indicated that GST-Nuf2-(1–385) undergoes severe proteolytic degradation, and that it is stabilized by its interaction with His-Hec1-(1–445) (compare *lanes 6* in *panels B* and *C*). Finally, we failed to detect binding between the predicted N-terminal globular heads of Nuf2 and Hec1, GST-Nuf2-(1–137) and His-Hec1-(1–230) (not shown). In summary, the entire length of the coiled coils of Hec1 and Nuf2 is engaged in dimerization.

The same approach was applied to Spc24-Spc25. First, we tested the ability of a His-tagged version of the N-terminal region of Spc25 (His-Spc25-(1–144)) to bind GST-tagged versions of the N- or C-terminal regions of Spc24 (GST-Spc24-(1–131) or GST-Spc24-(132–197)). His-Spc25-(1–144) bound tightly to GST-Spc24-(1–131) (Fig. 1*D*, *lane 6*). His-Spc25-(1–144) also bound reproducibly to GST-Spc24-(132–197) (Fig. 1*D*, *lane 9*), but this may be an artifact caused by the instability of GST-Spc24-(132–197), which undergoes severe proteolytic degradation. Next, we tested the predicted C-terminal globular domain of Spc25 (His-Spc25-(145–224)) against GST-Spc24-(1–131) and GST-Spc24-(132–197). His-Spc25-(145–224) bound weakly to GST-Spc24-(132–197) (Fig. 1*E*, *lane 9*). As explained above, this might also be an artifact caused by the instability of GST-Spc24-(132–197). However, at least a fraction of GST-Spc24-(132–197) was protected from degradation upon co-expression with His-Spc25-(145–224), suggesting that the latter stabilizes Spc24-(132–197) presumably because it binds to it. No binding was observed between His-Spc25-(145–224) and GST-Spc24-(1–131). As for Nuf2 and Hec1, the binding studies with Spc24 and Spc25 suggest that the interaction between these proteins involves coiled coil domains organized in a co-linear and parallel arrangement (see "Discussion").

Domains Required for Tetramerization of the Ndc80 Complex—Next, we sought to identify the domains in the Spc24-Spc25 and Nuf2-Hec1 subcomplexes responsible for tetramerization of the Ndc80 complex. We tested to determine if Nuf2-(1–385)·Hec1-(1–445) and Nuf2-(386–464)·Hec1-(446–642), stable dimeric partners of Nuf2-Hec1 (Fig. 1), bound full-length Spc24-Spc25 or Spc24-(70–197)·Spc25-(57–224), a stable dimeric fragment of Spc24-Spc25 identified by limited proteolysis (data not shown). All dimeric constructs were generated by co-expression in *E. coli* and purified on GSH-Sepharose beads. After release from the GST moiety by protease cleavage, the samples were analyzed by SEC on a Superdex 200 column as shown in Fig. 2, *A–D*. To facilitate the interpretation of the SEC profiles, we covalently labeled full-length Spc24-Spc25 and Spc24-(70–197)·Spc25-(57–224) with the fluorophore Alexa Fluor 488 to track elution at both 280 and 495 nm. The elution profiles of the individual dimeric constructs Alexa-Spc24-Spc25, Spc24-(70–197)·Spc25-(57–224), Nuf2-(1–385)·Hec1-(1–445), and Nuf2-(386–464)·Hec1-(446–642) are shown in Fig. 2, *A–D* for reference.

To identify the domains linking Hec1-Nuf2 to Spc24–25, we mixed roughly stoichiometric amounts of each purified dimer for 2 h at 4 °C. SEC analysis of the resulting products revealed that Nuf2-(1–385)·Hec1-(1–445) was unable to bind full-length Spc24-Spc25 or Spc24-(70–197)·Spc25-(57–224). In both cases, the dimeric fragments eluted separately with unaltered elution volumes relative to those of the isolated dimers (Fig. 2, *E* and *F*). On the other hand, Nuf2-(386–464)·Hec1-(446–642) bound full-length Alexa-Spc24-Spc25. The four proteins eluted together in a single peak, the elution volume of which was significantly smaller relative to that of the individual dimeric constituents, indicative of a larger Stokes radius (Fig. 2*G*). Using a similar analysis, we found that Nuf2-(386–464)·Hec1-(446–642) was unable to form a tetramer when mixed with the Spc24-(70–197)·Spc25-(57–224) subcomplex, indicating that the N-terminal regions of Spc24 and Spc25 missing from this construct are necessary for the tetramerization of the Ndc80 complex (Fig. 2*H*). Thus, our studies identify the dimeric fragment containing the C-terminal segments of Nuf2-Hec1 as being sufficient to mediate the formation of a tetramer with Spc24-Spc25, whose N-terminal regions are necessary for binding.

Reconstitution of the Ndc80 Complex—The dicistronic configurations Hec1-Nuf2 and Spc24-Spc25, described above, were used successfully to express soluble full-length subcomplexes of Ndc80 tagged with GST or a His tag (Fig. 3, *A* and *B*; Spc25 and Spc24 appear to co-migrate in this gel, and the same happens for Hec1 and GST-Nuf2). Co-expression generated soluble complexes that could be purified using affinity chromatography and SEC. With no other combination of subunits we obtained stable subcomplexes that rescue the insolubility of the individual subunits (data not shown), confirming that Nuf2-Hec1 and Spc24-Spc25 represent physically well defined subcomplexes.

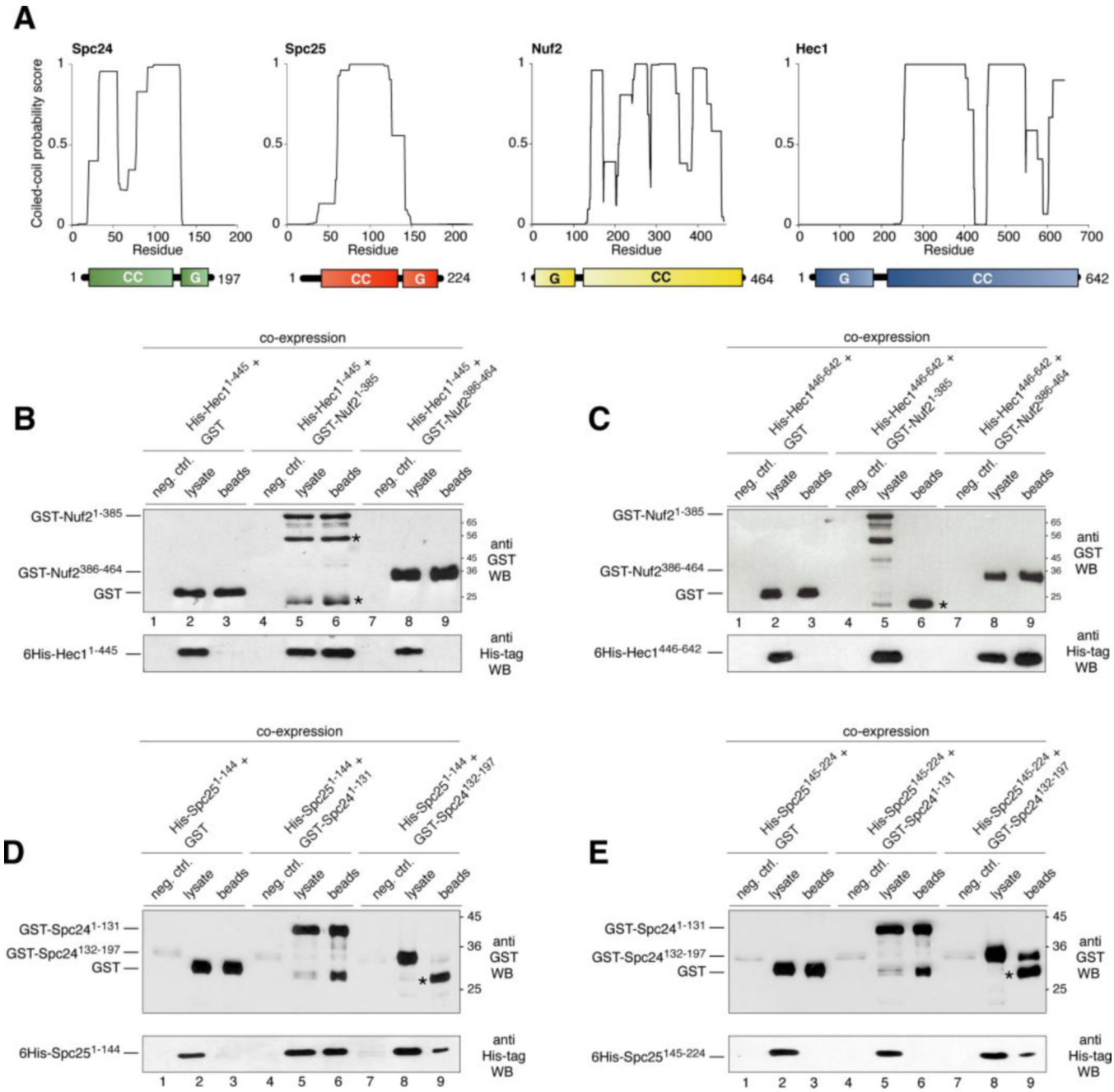

FIG. 1. **Identification of subcomplexes of the Ndc80 complex.** *A*, coiled coil predictions (40) for subunits of human Ndc80 complex (window = 21) are shown together with a schematic view of domains. *CC*, coiled coil; *G*, globular domain. *B*, His-Hec1-(1–445) was co-expressed with GST or GST fusions of N- or C-terminal segments of Nuf2. Cells were lysed, and GST proteins were affinity-purified on GSH-Sepharose beads. Lysate and bound fractions were separated by SDS-PAGE. His-Hec1-(1–445) was detected by WB with an anti-His tag antibody. Control anti-GST WBs are also shown. The *asterisk*s mark bands reactive to the anti-GST antibody in *lanes 5* and *6* that presumably result from the degradation of GST-Nuf2-(1–385). The *bottom band* migrates faster than GST, suggesting that the fusion might slightly perturb the stability of GST, causing its partial degradation. *C*, as in *panel B*, but with His-Hec1-(446–642) rather than His-Hec1-(1–445). The *asterisk* marks a degradation product of GST-Nuf2-(1–385). Note that in *panel B* GST-Nuf2-(1–385) is partly protected from degradation through its binding to His-Hec1-(1–445) (*lane 6*) When no binding occurs, as in *lane 6* of *panel C*, the segment is unstable and degraded. *D*, His-Spc25-(1–144) was co-expressed with GST or GST fusions of N- or C-terminal segments of Spc24. Binding was detected as in *panel B*. The *asterisk* marks a prominent degradation product of GST-Spc24-(132–197). *E*, as in *panel D*, but with His-Spc25-(145–224). The *asterisk* is the same as in *panel D*. *neg. ctrl.*, negative control; *6His*, His_6.

To reconstitute the quaternary Ndc80 complex, we typically expressed GST-Spc24-Spc25 and GST-Nuf2-Hec1 separately and purified them by affinity chromatography on GSH-Sepharose beads. While still bound onto the beads, the Spc24-Spc25 was removed from the GST moiety by proteolytic cleavage and subsequently incubated with limiting amounts of GST-Nuf2-Hec1 immobilized on beads. After removing the excess Spc24-Spc25, the resulting GST-Nuf2-Hec1-Spc24-Spc25 complex was released from beads by proteolysis, concentrated by ultrafiltration, and analyzed by SEC on a Superose 6 PC 3.2/30 column (Fig. 3*C*). The SEC elution profile revealed a single prominent peak with an elution volume corresponding to an apparent molecular mass of ~700–800 kDa. SDS-PAGE analysis revealed that the peak contained all four subunits of the Ndc80 complex in a pure form and in apparently stoichiometric proportions (Fig. 3*C*).

We wished to know if the Stokes radius of the endogenous human Ndc80 complex was comparable with that of the recom-

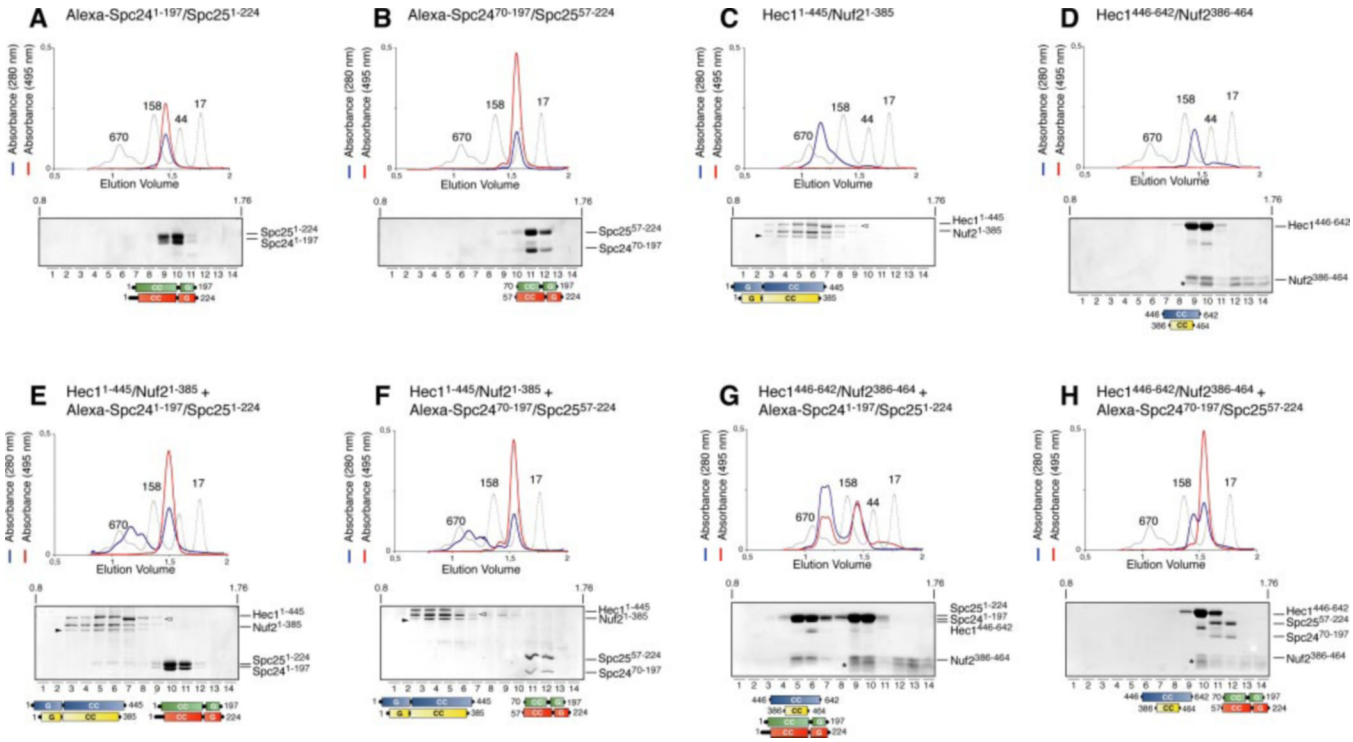

FIG. 2. **Identification of a domain for Ndc80 complex tetramerization.** The indicated samples were analyzed by SEC on a Superdex-200 PC 3.2/30 column (see "Materials and Methods"). The content of 14 33-μl fractions representing every second fraction in the range 0.8–1.76 ml is shown in Coomassie-stained SDS-PAGE gels. Red profiles report Alexa Fluor 488 absorbance at 495 nm. *A*, elution profile of Alexa-Spc24-(1–197)·Spc25-(1–224) (full-length). *B*, Alexa-Spc24-(70–197)·Spc25-(57–224). *C*, Hec1-(1–445)·Nuf2-(1–385). *D*, Hec1-(446–642)·Nuf2-(386–464). *E*, stoichiometric amounts of Hec1-(1–445)·Nuf2-(1–385) and Alexa-Spc24-(1–197)·Spc25-(1–224) were incubated at 4 °C for 2 h prior to SEC analysis. Elution of the two subcomplexes is unaltered, indicating lack of binding. *F*, Hec1-(1–445)·Nuf2-(1–385) and Alexa-Spc24-(70–197)·Spc25-(57–224) were analyzed as in *panel E* and failed to bind. *G*, binding of Hec1-(446–642)·Nuf2-(386–464) and Alexa-Spc24-(1–197)·Spc25-(1–224) is revealed by a prominent shift toward the larger Stokes radius of the Alexa signal. *H*, Hec1-(446–642)·Nuf2-(386–464) and Alexa-Spc24-(70–197)·Spc25-(57–224) do not bind. The *black* and *white arrowheads* and the *asterisk* indicate recurrent degradations products of the Hec1-(1–445)·Nuf2-(1–385) and Hec1-(446–642)·Nuf2-(386–464) constructs, respectively. *CC*, coiled coil; *G*, globular domain.

binant complex. For this question we lysed cycling HeLa cells, separated the lysate by SEC on the same Superose 6 PC 3.2/30 column, and analyzed different fractions of the eluate by WB with an anti-Hec1 antibody (Fig. 3*D*). The elution profile of endogenous Hec1, which we assume to be part of a larger complex with Nuf2, Spc24, and Spc25, was essentially identical to that of the recombinant Ndc80 complex (shown in Fig. 3*C*), suggesting that the recombinant and endogenous Ndc80 complexes have similar Stokes radii.

Hydrodynamic Characterization of the Ndc80 Complex—Because the predicted molecular mass of the Ndc80 complex is 176 kDa (assuming a 1:1:1:1 stoichiometry), its elution volume suggested the possibility that the complex forms higher oligomers. However, because all four subunits of Ndc80 are probably elongated because of a high content of coiled coil structure, the Stokes radius of the complex (and therefore its elution volume) may deviate significantly from that expected for a globular protein of equivalent molecular mass.

The Stokes radius of recombinant Ndc80 was derived from a calibration curve of SEC elution volume and determined to be ~90 Å (see "Materials and Methods"). This result is very similar to the 87-Å value proposed for the endogenous Ndc80 complex in budding yeast (10). Next, we determined the sedimentation behavior of the Ndc80 complex using glycerol density gradients (5–40%). This experiment returned a sedimentation coefficient of ~4.8 S (Fig. 3*E*). With these values we used the Siegel and Monty equation (36) to calculate the molecular mass of the recombinant Ndc80 complex and obtained a value of 177 kDa, in excellent agreement with the predicted molecular mass of ~176 kDa. Thus, the combination of SEC and sedimentation in glycerol gradients allowed us to conclude that the recombinant Ndc80 complex is a stoichiometric 1:1:1:1 complex with a molecular mass of 177 kDa. To confirm that the endogenous Ndc80 complex sediments similarly to the recombinant one, we subjected cell lysates from cycling HeLa cells to sedimentation in glycerol density gradients and analyzed the resulting fractions by WB with an anti-Hec1 antibody. As shown in Fig. 3*F*, the sedimentation properties of endogenous Ndc80 were indistinguishable from those of the recombinant complex, indicating that the recombinant complex is a faithful copy of the endogenous Ndc80 complex. Overall, these studies show that the human Ndc80 complex is very elongated. The hydrodynamic parameters of the recombinant and endogenous human Ndc80 complexes indicate that this type of complex can be modeled as a prolate ellipsoid of revolution with the axial ratio $a/b = 21$ (Fig. 3*G*). Similar values have been recently reported for the endogenous Ndc80 complexes of *S. cerevisiae* and *Xenopus laevis* (10, 24).

The Recombinant Ndc80 Complex Localizes to Kinetochores—We tried to corroborate the idea that the recombinant complex represents a good model for the endogenous complex, asking if it was capable of reaching the mitotic kinetochore when injected in PtK1 or HeLa cells. Toward this end, we covalently labeled the Spc24-Spc25 subcomplex with Alexa Fluor 488. Alexa-Spc24-Spc25 was used either directly for injection or to reconstitute a fluorescent version of the entire Ndc80 complex. For this experiment the fluorescently labeled Spc24-Spc25 subcomplex was mixed with solid phase bound GST-Nuf2-Hec1, and the resulting complex was further purified as described above for the unlabeled complex.

Prophase PtK1 or mitotic HeLa cells were microinjected with 1–5% cell volume of the Alexa-labeled Spc24-Spc25 complex

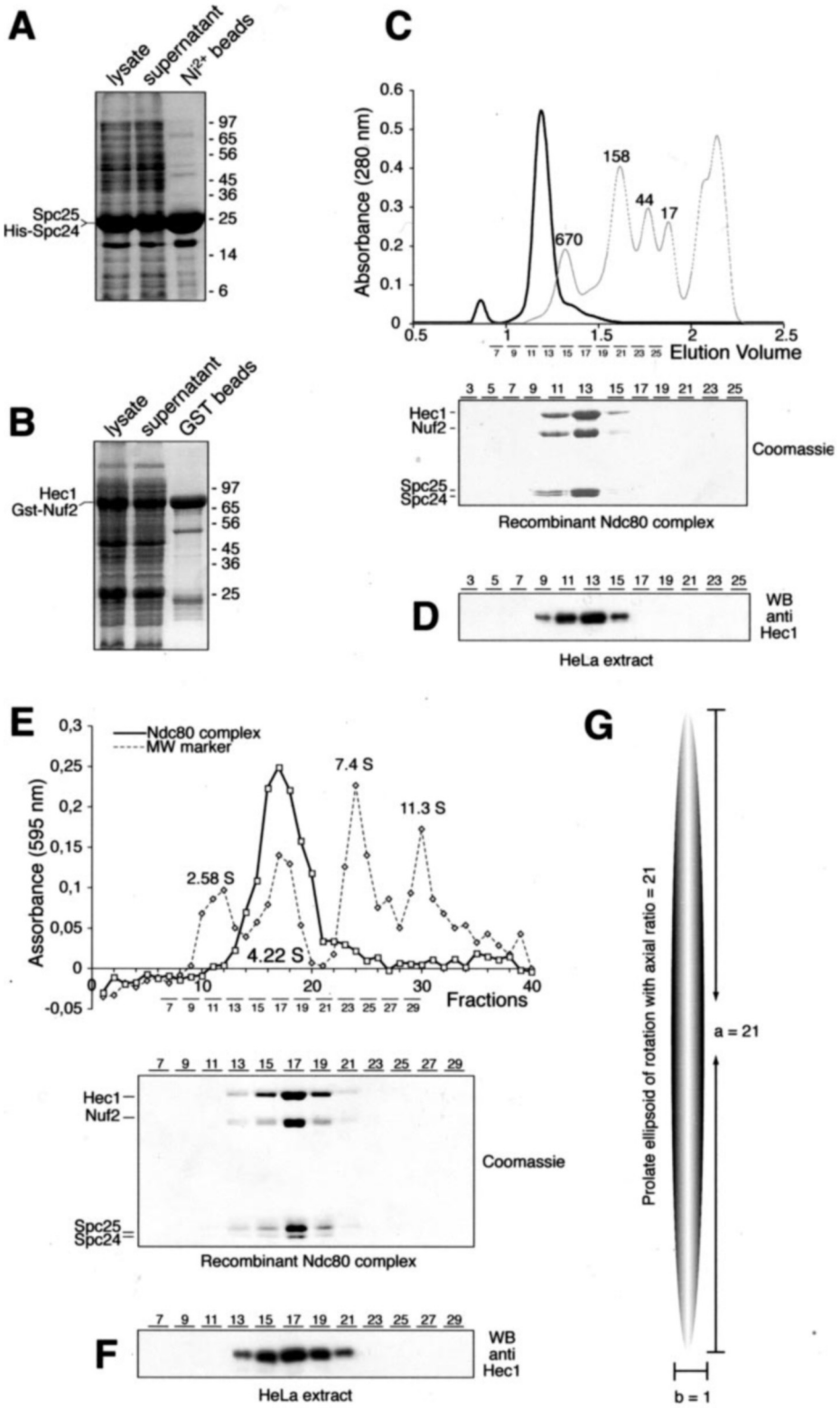

FIG. 3. **Hydrodynamic analysis of recombinant and endogenous Ndc80 complex.** *A*, co-expression of His-Spc24-Spc25 and its purification by metal affinity chromatography. *B*, co-expression of GST-Nuf2-Hec1 and its purification on GSH-Sepharose beads. *C*, elution profile of a reconstituted Ndc80 complex from a Superdex 200 PC 3.2/30 column and a Coomassie-stained SDS-PAGE showing the content of the indicated fractions. *D*, elution profile of an endogenous HeLa Ndc80 complex from the same column revealed by WB with an anti-Hec1 antibody. *E*, sedimentation analysis of the recombinant Ndc80 complex on a 5–40% glycerol gradient and Coomassie-stained SDS-PAGE of fractions through the gradient. *F*, anti-Hec1 WB of fractions from the sedimentation analysis of HeLa cells lysates. *G*, the prolate ellipsoid of revolution obtained by rotating an ellipse about its long axis, *a* (*a*/*b* = 21; see "Results").

(needle concentration of 86 μM) or Alexa-labeled Hec1 complex (needle concentration of 26 μM) and analyzed by live cell fluorescence microscopy (Fig. 4). Imaging was started ~15 min post-injection. Of nine prophase PtK1 cells injected with Alexa-Spc24-Spc25, nine showed strong kinetochore localization (Fig. 4*A*). Similarly, we injected 16 mitotic HeLa cells with Alexa-Spc24-Spc25, and all 16 showed strong kinetochore localization (Fig. 4*C*). We also injected three prophase PtK1 and 11 HeLa mitotic cells with the Alexa-Ndc80 complex, and all cells showed strong kinetochore localization (Fig. 4, *B* and *D*). Injected HeLa cells completed mitosis normally, indicating that the injected complexes do not interfere with normal kinetochore function (not shown).

Organization of the Ndc80 Complex as Imaged by Scanning Force Microscopy—We obtained images of individual recombinant Ndc80 complexes using scanning force microscopy (SFM). SFM revealed an elongated structure with an overall length of 40–45 nm (Fig. 5*A*). Two globular regions are located at each

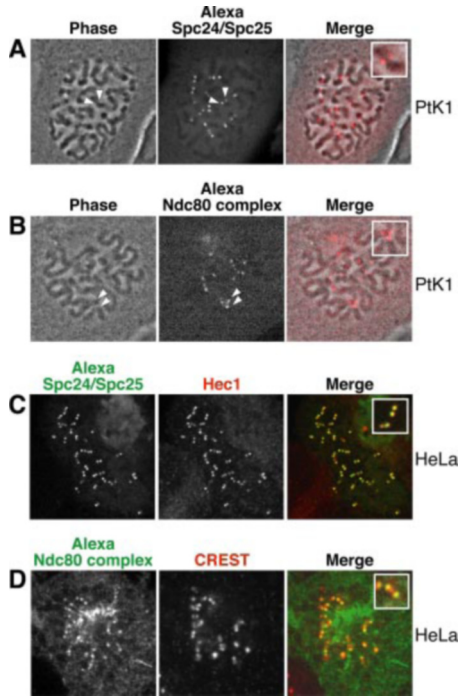

FIG. 4. **Localization of Hec1 and Spc24-Spc25 subcomplexes at the kinetochore.** *A* and *B*, prophase PtK1 cells were injected with Alexa-labeled Spc24-Spc25 subcomplex (*A*) or Alexa-labeled Ndc80 complex (*B*) and imaged by live cell fluorescence microscopy. Strong kinetochore staining is observed. Phase contrast (*left*), fluorescence (*center*), and merged images (*right*) are shown. *C* and *D*, mitotic HeLa cells were injected with Alexa-labeled Spc24-Spc25 subcomplex (*C*) or Alexa-labeled Hec1-Nuf2-Spc24-Spc25 (*D*). After injection, cells were either filmed by live cell fluorescence microscopy (not shown) or fixed. In *panel C* the localization of Alexa-labeled Spc24-Spc25 is shown together with that of endogenous Hec1 as revealed by indirect immunofluorescence. The *right section* shows perfect co-localization of the two signals. In *panel D* the signal from Alexa-labeled Hec1-Nuf2-Spc24-Spc25 is compared with that of CREST, a centromeric marker. As expected, the kinetochore signal of the Ndc80 complex lies at two bright dots external to CREST (see *inset*).

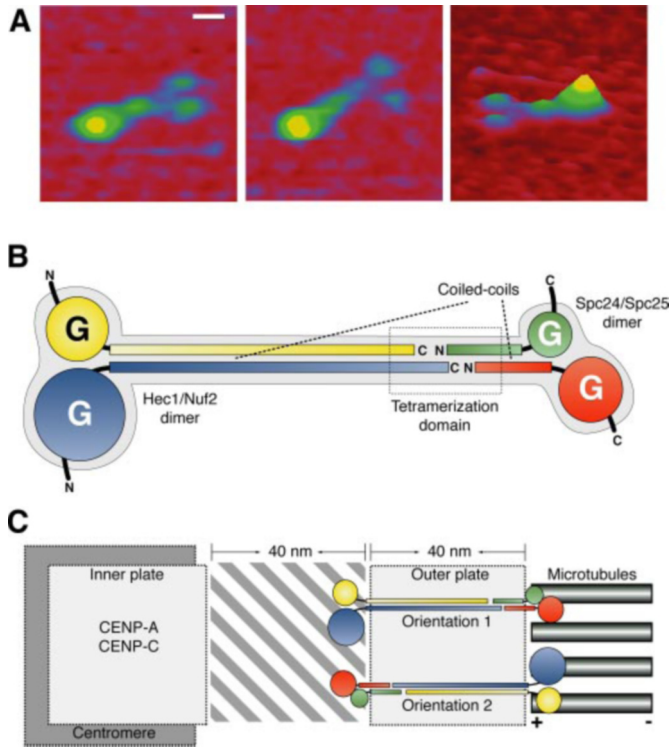

FIG. 5. **Summary of structural features of the Ndc80 complex.** *A*, zoom (*left* and *middle*) and tilt (*right*) images of individual Ndc80 complexes imaged by SFM. Two globular regions are located at each end of a central shaft. The *white bar* corresponds to 10 nm. *B*, the elongated Ndc80 complex contains globular regions at each end of a central shaft containing the coiled coils of the Hec1-Nuf and Spc24-Spc5 subcomplexes. The tetramerization domain is proposed to involve the C termini of the Hec1-Nuf2 coiled coil and the N termini of the Spc24-Spc25 coiled coils. The bridge between subcomplexes might consist of overlapping C- and N-terminal segments of Hec1 and Spc24, respectively, as these may be unpaired to the Nuf2 and Spc25 chains, respectively (see "Discussion"). *C*, an ~40-nm gap of unknown composition separates the inner plate of the kinetochore from the outer plate. Microtubule plus ends terminate on the outer plate. The fibrous corona (not shown) is only visible on unattached kinetochores and may be altered after microtubule arrival (1). Two possible orientations of the Ndc80 complex are shown.

end of a central shaft. With the preliminary word of caution that dimensions are rather distorted in SFM images and only allow relative rather than absolute size assessments, the height of the larger blob is ~9–10 nm, and that of the central shaft and the opposite end is 3–4-nm-high. Based on the fact that the predicted globular regions of Hec1-Nuf2 are significantly larger than those of Spc24-Spc25 (Fig. 1), we suspect that the larger blob corresponds to the globular regions at the N termini of the Hec1-Nuf2 subcomplex. The smaller globular region at the opposite end of the shaft appears to be split into two distinct blobs of density. If our assignment of domains is correct, this observation predicts that the C-terminal globular domains of Spc24-Spc24 are separated, an unexpected finding based on our binding studies in Fig. 1 that will require further future investigations.

DISCUSSION

Our results have interesting implications for understanding the overall organization of the Ndc80 complex. At the resolution of our analysis, the dimerization interfaces we identified coincide with the coiled coil regions of Nuf2 and Hec1. The colinearity of the interaction suggests that the intermolecular coiled coil of Hec1 and Nuf2 is parallel. This organization explains why Hec1 and Nuf2 are mutually dependent on their stability (see, for instance, Refs. 28 and 33). Spc24 and Spc25, on the other hand, are predicted to contain relatively short N-terminal coiled coils and small C-terminal globular domains, and also in this case we observed colinearity of the heterodimerization interface. The colinearity of the Hec1-Nuf2 and Spc24-Spc25 subcomplexes is consistent with the observed Stokes radii for different segments of the complex, which increase with an imperfect but consistent additive rule with increasing protein size. For instance, Spc24-(70–197)·Spc25-(57–224) and full-length Spc24-Spc25 have Stokes radii of 28 and 37 Å, respectively, whereas Nuf2-(386–464)·Hec1-(446–642) and Nuf2-(1–385)·Hec1-(1–445) have Stokes radii of 42 and 65 Å, respectively (data not shown). The full-length quaternary complex has a Stokes radius of 90 Å. This suggests that the different sub-domains of the Ndc80 complex extend linearly to build a progressively more elongated shape. The tetramerization of the Nuf2-Hec1 and Spc24-Spc25 subcomplexes is mediated by the encounter of the C-terminal regions of Nuf2-Hec1 and the N-terminal regions of Spc24-Spc25. We failed to observe interactions between other portions of these subcomplexes, suggesting that the tetramerization domain involves a relatively small portion of the Ndc80 complex.

This information can be nicely fitted into the shape of the Ndc80 complex imaged by SFM. We predict that the parallel coiled coil of Hec1-Nuf2 contributes the most prominent fraction of the central shaft. It also accommodates the tetramerization domain and the N-terminal coiled coil of Spc24-Spc25. In the absence of high resolution structural information, it is difficult to say whether the coiled coil regions of Hec1-Nuf2 and

Spc24-Spc25 extend in a single direction or whether they invert their direction, creating a more complex pattern. The paired coiled coil segment of the Hec1-Nuf2 subcomplex may extend for 250–300 residues, allowing for 75–85 helical turns and a predicted length of 40–45 nm, similar to the length of the complex imaged by SFM. Assuming that the pairing of the Nuf2 and Hec1 coiled coils starts at their N-terminal ends, an overhang containing the C terminus of Hec1 is expected (Fig. 5*B*). We postulate that this overhang might mediate the interaction with the N-terminal regions of Spc24-Spc25. By limited proteolysis, we found that the N-terminal regions of the Spc24-Spc25 subcomplex are unstable in the absence of Hec1-Nuf2 (data not shown). In these experiments, longer N-terminal segments of Spc24 are removed relative to Spc25, suggesting that the N-terminal region of Spc24 has unpaired regions that might mediate pairing of Spc24-Spc25 with Nuf2-Hec1. We also expect that the opposing globular regions flanking the central shaft contain the N termini of the Hec1-Nuf2 subcomplex and the C termini of Spc24-Spc25, respectively (Fig. 5*B*). This organization is similar to that very recently proposed for the Ndc80 complex of *S. cerevisiae* (41).

The length of the Ndc80 complex is very close to the 40-nm thickness attributed to the kinetochore outer plate (13–18). The model is compatible with (but does not imply) the possibility that the Ndc80 complex orients perpendicularly to the kinetochore outer surface, accounting for the whole thickness of the outer plate (Fig. 5*C*). Of note, other evolutionarily conserved kinetochore complexes interacting with the Ndc80 complex, such as the Mtw1-Mis12 complex, have been proposed to be elongated and might adopt a similar orientation in the kinetochore outer plate (10). Important questions raised by this model regard the positioning of the opposing globular ends and the identity of their binding partners. Our injection studies with fluorescent constructs show that Spc24-Spc25 reaches its normal kinetochore localization in the absence of Hec1-Nuf2 (Fig. 4). The injected cells completed mitosis normally, suggesting the possibility that the injected Spc24-Spc25 subcomplex is normally incorporated in the larger Ndc80 assembly or that it does not interfere with kinetochore function if recruited to kinetochores independently of Hec1-Nuf2. We asked if Hec1-Nuf2 was required for kinetochore recruitment of Spc24-Spc25 by injecting HeLa cells with Alexa-Spc24-(70–197)·Spc25-(57–224), which is unable to bind Hec1-Nuf2. Kinetochore localization of Spc24-(70–197)·Spc25-(57–224) was dramatically reduced relative to that of the full-length Spc24-Spc25 subcomplex shown in Fig. 4 (not shown). The experiment, however, was not conclusive, because some faint but recognizable kinetochore decoration was still visible in a subset of injected cells.

The recombinant Ndc80 complex is endowed with all known properties of the endogenous Ndc80 complex. Our results underscore the relevance of biochemical reconstitution strategies to combine the study of complex protein behavior *in vitro* and in living cells. We tested the ability of recombinant Ndc80 to bind recombinant segments of Mad1, a spindle checkpoint component indicated as a possible binding partner of the Hec1 and Spc25 subunits (31, 42). To date, however, we have failed to detect a direct interaction between Mad1 and the Ndc80 complex (not shown). In the future, we plan to test the interaction of the Ndc80 complex with its partners at the kinetochore, dissect the requirements for its recruitment to kinetochores, and understand its contributions to microtubule binding.

Acknowledgments—We thank Lucia Massimiliano for assistance and all members of the Musacchio Laboratory for discussions.

REFERENCES

1. Cleveland, D. W., Mao, Y., and Sullivan, K. F. (2003) *Cell* **112,** 407–421
2. Amor, D. J., Kalitsis, P., Sumer, H., and Choo, K. H. (2004) *Trends Cell Biol.* **14,** 359–368
3. McAinsh, A. D., Tytell, J. D., and Sorger, P. K. (2003) *Annu. Rev. Cell Dev. Biol.* **19,** 519–539
4. Musacchio, A., and Hardwick, K. G. (2002) *Nat. Rev. Mol. Cell Biol.* **3,** 731–741
5. Pinsky, B. A., Tatsutani, S. Y., Collins, K. A., and Biggins, S. (2003) *Dev. Cell* **5,** 735–745
6. Hayashi, T., Fujita, Y., Iwasaki, O., Adachi, Y., Takahashi, K., and Yanagida, M. (2004) *Cell* **118,** 715–729
7. Obuse, C., Iwasaki, O., Kiyomitsu, T., Goshima, G., Toyoda, Y., and Yanagida, M. (2004) *Nat. Cell Biol.* **6,** 1135–1141
8. Nekrasov, V. S., Smith, M. A., Peak-Chew, S., and Kilmartin, J. V. (2003) *Mol. Biol. Cell* **14,** 4931–4946
9. Cheeseman, I. M., Niessen, S., Anderson, S., Hyndman, F., Yates, J. R., III, Oegema, K., and Desai, A. (2004) *Genes Dev.* **18,** 2255–2268
10. De Wulf, P., McAinsh, A. D., and Sorger, P. K. (2003) *Genes Dev.* **17,** 2902–2921
11. Westermann, S., Cheeseman, I. M., Anderson, S., Yates, J. R., III, Drubin, D. G., and Barnes, G. (2003) *J. Cell Biol.* **163,** 215–222
12. Desai, A., Rybina, S., Muller-Reichert, T., Shevchenko, A., Hyman, A., and Oegema, K. (2003) *Genes Dev.* **17,** 2421–2435
13. McEwen, B. F., Heagle, A. B., Cassels, G. O., Buttle, K. F., and Rieder, C. L. (1997) *J. Cell Biol.* **137,** 1567–1580
14. Yao, X., Anderson, K. L., and Cleveland, D. W. (1997) *J. Cell Biol.* **139,** 435–447
15. Rieder, C. L. (1982) *Int. Rev. Cytol* **79,** 1–58
16. Jokelainen, P. T. (1967) *J. Ultrastruct. Res.* **19,** 19–44
17. McEwen, B. F., Arena, J. T., Frank, J., and Rieder, C. L. (1993) *J. Cell Biol.* **120,** 301–312
18. Cooke, C. A., Schaar, B., Yen, T. J., and Earnshaw, W. C. (1997) *Chromosoma* **106,** 446–455
19. Maiato, H., Deluca, J., Salmon, E. D., and Earnshaw, W. C. (2004) *J. Cell Sci.* **117,** 5461–5477
20. Kline-Smith, S. L., Sandall, S., and Desai, A. (2005) *Curr. Opin. Cell Biol.* **17,** 35–46
21. Wigge, P. A., and Kilmartin, J. V. (2001) *J. Cell Biol.* **152,** 349–360
22. Janke, C., Ortiz, J., Lechner, J., Shevchenko, A., Magiera, M. M., Schramm, C., and Schiebel, E. (2001) *EMBO J.* **20,** 777–791
23. Bharadwaj, R., Qi, W., and Yu, H. (2003) *J. Biol. Chem.* **279,** 13076–13085
24. McCleland, M. L., Gardner, R. D., Kallio, M. J., Daum, J. R., Gorbsky, G. J., Burke, D. J., and Stukenberg, P. T. (2003) *Genes Dev.* **17,** 101–114
25. McCleland, M. L., Kallio, M. J., Barrett-Wilt, G. A., Kestner, C. A., Shabanowitz, J., Hunt, D. F., Gorbsky, G. J., and Stukenberg, P. T. (2004) *Curr. Biol.* **14,** 131–137
26. Chen, Y., Riley, D., Chen, P., and Lee, W. (1997) *Mol. Cell. Biol.* **17,** 6049–6056
27. Howe, M., McDonald, K. L., Albertson, D. G., and Meyer, B. J. (2001) *J. Cell Biol.* **153,** 1227–1238
28. DeLuca, J. G., Howell, B. J., Canman, J. C., Hickey, J. M., Fang, G., and Salmon, E. D. (2003) *Curr. Biol.* **13,** 2103–2109
29. DeLuca, J. G., Moree, B., Hickey, J. M., Kilmartin, J. V., and Salmon, E. D. (2002) *J. Cell Biol.* **159,** 549–555
30. DeLuca, J. G., Dong, Y., Hergert, P., Strauss, J., Hickey, J. M., Salmon, E. D., and McEwen, B. F. (2005) *Mol. Biol. Cell* **16,** 519–531
31. Martin-Lluesma, S., Stucke, V. M., and Nigg, E. A. (2002) *Science* **297,** 2267–2270
32. Hori, T., Haraguchi, T., Hiraoka, Y., Kimura, H., and Fukagawa, T. (2003) *J. Cell Sci.* **116,** 3347–3362
33. Meraldi, P., Draviam, V. M., and Sorger, P. K. (2004) *Dev. Cell* **7,** 45–60
34. Gillett, E. S., Espelin, C. W., and Sorger, P. K. (2004) *J. Cell Biol.* **164,** 535–546
35. Nabetani, A., Koujin, T., Tsutsumi, C., Haraguchi, T., and Hiraoka, Y. (2001) *Chromosoma* **110,** 322–334
36. Siegel, L. M., and Monty, K. J. (1966) *Biochim. Biophys. Acta* **112,** 346–362
37. Harding, S. E., and Colfen, H. (1995) *Anal. Biochem.* **228,** 131–142
38. De Antoni, A., Pearson, C. G., Cimini, D., Canman, J. C., Sala, V., Nezi, L., Mapelli, M., Sironi, L., Faretta, M., Salmon, E. D., and Musacchio, A. (2005) *Curr. Biol.* **15,** 214–225
39. Howell, B. J., Hoffman, D. B., Fang, G., Murray, A. W., and Salmon, E. D. (2000) *J. Cell Biol.* **150,** 1233–1250
40. Lupas, A., Van Dyke, M., and Stock, J. (1991) *Science* **252,** 1162–1164
41. Wei, R. R., Sorger, P. K., and Harrison, S. C. (2005) *Proc. Natl. Acad. Sci. U. S. A.* **102,** 5363–5367
42. Newman, J. R., Wolf, E., and Kim, P. S. (2000) *Proc. Natl. Acad. Sci. U. S. A.* **97,** 13203–13208